Molecular Therapy
Oncology
Original Article

Deletion of the RGD motif from the penton base in oncolytic adenoviruses enhances antitumor efficacy of combined CAR T cell therapy

Alvaro Morales-Molina,[1] Miguel Angel Rodriguez-Milla,[1] Patricia Garcia-Rodriguez,[1,2] Laura Hidalgo,[1] Ramon Alemany,[3] and Javier Garcia-Castro[1,4]

[1]Cellular Biotechnology Unit, Instituto de Salud Carlos III, 28220 Madrid, Spain; [2]Universidad Nacional de Educación a Distancia, UNED, 28015 Madrid, Spain; [3]Oncobell and ProCure Programs, IDIBELL-Institut Català d'Oncologia, L'Hospitalet de Llobregat, 08908 Barcelona, Spain; [4]Instituto de Investigación de Enfermedades Raras (IIER) & Departamento de Desarrollo de Medicamentos de Terapias Avanzadas (DDMTA), Instituto de Salud Carlos III, 28220 Madrid, Spain

Oncolytic viruses often face challenges in achieving optimal antitumor immunity as standalone therapies. The penton base RGD-integrin interactions play a significant role in wild-type adenovirus-induced innate immune responses. To modify these responses, we present ISC301, a novel oncolytic adenovirus engineered by deleting the natural RGD motifs in the penton base while incorporating artificial RGD motifs in the fiber knobs. ISC301 demonstrated comparable *in vitro* infectivity, cytotoxic effects, and signaling profiles across various cell types to its parental ICOVIR-5, which retains the penton base RGD motif. In immunodeficient and immunocompetent mouse models, ISC301 exhibited similar *in vivo* antitumor efficacy to ICOVIR-5. However, ISC301 induced higher intratumoral inflammation through NF-κB activation, leading to increased levels of tumor-infiltrating leukocytes and higher proportion of cytotoxic $CD8^+$ T cells. In addition, ISC301 elicits a heightened pro-inflammatory response in peripheral blood. Importantly, when combined with CAR T cell therapy, ISC301 exhibited superior antitumor efficacy, surpassing monotherapy outcomes. These findings emphasize the impact of adenoviral modifications on antitumor immune responses. The deletion of penton base RGD motifs enhances ISC301's pro-inflammatory profile and boosts CAR T cell therapy efficacy. This study enhances understanding of oncolytic virus engineering strategies, positioning ISC301 as a promising candidate for combined immunotherapeutic approaches in cancer treatment.

INTRODUCTION

Oncolytic viruses exhibit diverse mechanisms to eliminate cancer cells, including apoptosis, necrosis, and autophagy of infected cells; some of them classified as immunogenic cell death that may provoke potent and long-lasting anti-cancer immunity.[1] However, a limited antitumor immunity developed during virotherapy constrains the efficiency of oncolytic viruses when they are used as monotherapy.[2] In the same way, during its initial phases of chemotherapy, clinicians acknowledged that the most favorable results were achieved through the synergistic interplay of distinct drug combinations.[3,4] Conversely, in the contemporary landscape of immunotherapies, it is evident that the majority of monotherapies also encounter challenges in achieving clinical remissions.[5] Within this context, to further augment this efficacious response, oncolytic viruses have been genetically engineered to express immune regulators that enhance or restore antitumor immunity.[6] Furthermore, oncolytic viruses represent potential candidates to be used in combination with CAR T cell immunotherapy for the treatment of solid cancers.[7]

ICOVIR-5 and ICOCAV17 are human and canine oncolytic adenoviruses (OAds),[8–10] respectively, which have been successfully used in human and veterinary clinical trials based on a Trojan horse strategy known as Celyvir, wherein mesenchymal stem cells are infected with these OAds.[11–13] In our previous studies, we demonstrated a notable clinical efficacy and better clinical outcomes using this canine adenovirus (CAV), related with differences in intracellular signaling when compared with human adenovirus.[14] These findings led us to hypothesize that we could generate human adenoviruses with improved efficacy by mimicking specific attributes of CAVs.

It has been shown that canine adenovirus 2 vectors, which are based on wild-type CAV-2, induce a lower innate response than human adenovirus 5 (Ad5) vectors.[15] The same authors suggested that, although adenoviruses induce the innate immune response through various mechanisms, including complement activation, phagocytosis, and the induction of pro-inflammatory cytokines and interferons,[16,17] this response may be initiated by capsid endocytosis.[15] This process follows the low-affinity interaction between integrins and an arginine-glycine-aspartic acid (RGD) motif naturally present in the penton base protein of most human adenoviruses.[18] However, CAV-2 does not contain an RGD motif in the penton base, hexon, or fiber

Received 18 April 2024; accepted 20 August 2024;
https://doi.org/10.1016/j.omton.2024.200863.

Correspondence: Javier Garcia-Castro, Cellular Biotechnology Unit, Instituto de Salud Carlos III, 28220 Madrid, Spain.
E-mail: jgcastro@isciii.es

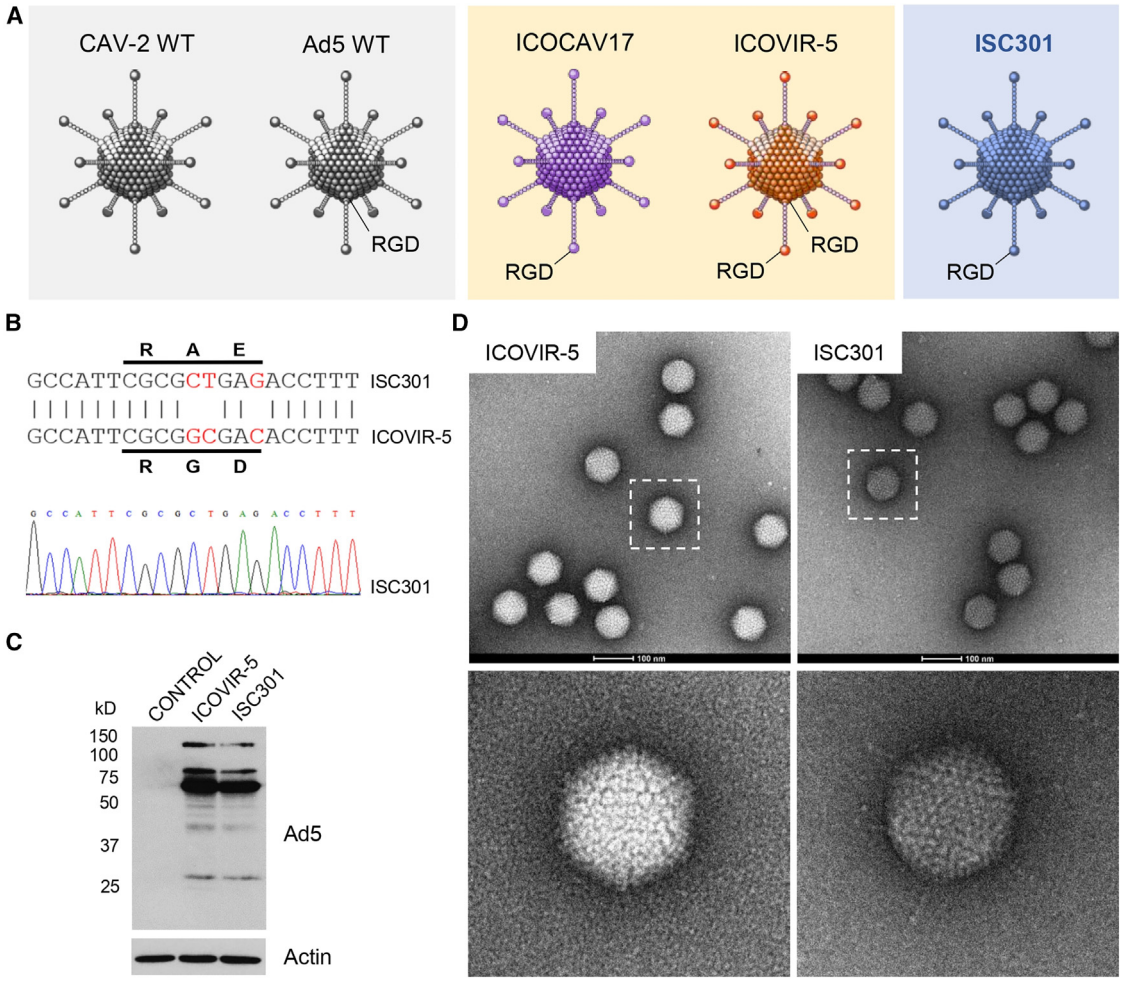

Figure 1. Design and engineering of ISC301

(A) Comparison of the RGD motifs presence or absence in the penton base and/or fiber of wild-type (WT) canine and human adenoviruses (gray background), canine ICOCAV17, and human ICOVIR-5 OAds (yellow background), and novel human OAd ISC301 (blue background). (B) Alignment of a fragment of the nucleotide sequence of ICOVIR-5 coding the penton base RGD motif with the homologous region of ISC301. Note the nucleotide mutations in ISC301 that result in the change of the RGD motif to the amino acid sequence RAE. The DNA sequence chromatogram showing the nucleotide mutations in ISC301 is shown at the bottom. (C) Western blot analysis showing the expression of adenoviral proteins in HEK293 cells infected for 24 h with ICOVIR-5 and ISC301 (200 PFU/cell). Actin was used as a loading control. (D) Transmission electron microscopy images of ICOVIR-5 and ISC301 (upper images), below details of the boxes with dashed line. Scale bar, 100 nm (upper images).

proteins.[19] Therefore, CAV-2 vectors may not activate the innate immune response in the same way as human adenoviruses do.[15]

Both human adenovirus species F (serotypes HAdV-40 and HAdV-41), which does not possess the RGD motifs,[20] and adenoviral vectors with penton base RGD motifs deleted have been designed resulting to be slightly less infectious,[21] and showing reduced CXCL10 activation and TNF-α expression.[21–23] These results suggest that RGD-integrin interactions play an important role in adenoviral induction of inflammatory genes. Thus, in this report, we engineered a novel human OAd called ISC301. Based on the background of ICOVIR-5, ISC301 presents the deletion of penton base RGD motifs, while maintaining artificial RGD motifs at the fiber knobs, a similar capsid structure regarding its RGD composition of canine ICOCAV17.

We show that ISC301 presents similar infectivity and cell signaling *in vitro* in several cell types compared with ICOVIR-5. Remarkably, in *in vivo* studies using our naked OAds administered intravenously, ISC301 demonstrated a surprising ability to induce higher intratumoral inflammation through the activation of the NF-κB pathway, resulting in an increase of tumor-infiltrating leukocytes. Taking advantage of this tumor-localized pro-inflammatory status, the combination of ISC301 with CAR T cell therapy exhibited higher antitumor efficacy compared with using ICOVIR-5 or CAR T as monotherapy. In conclusion, the deletion of the RGD motifs in the

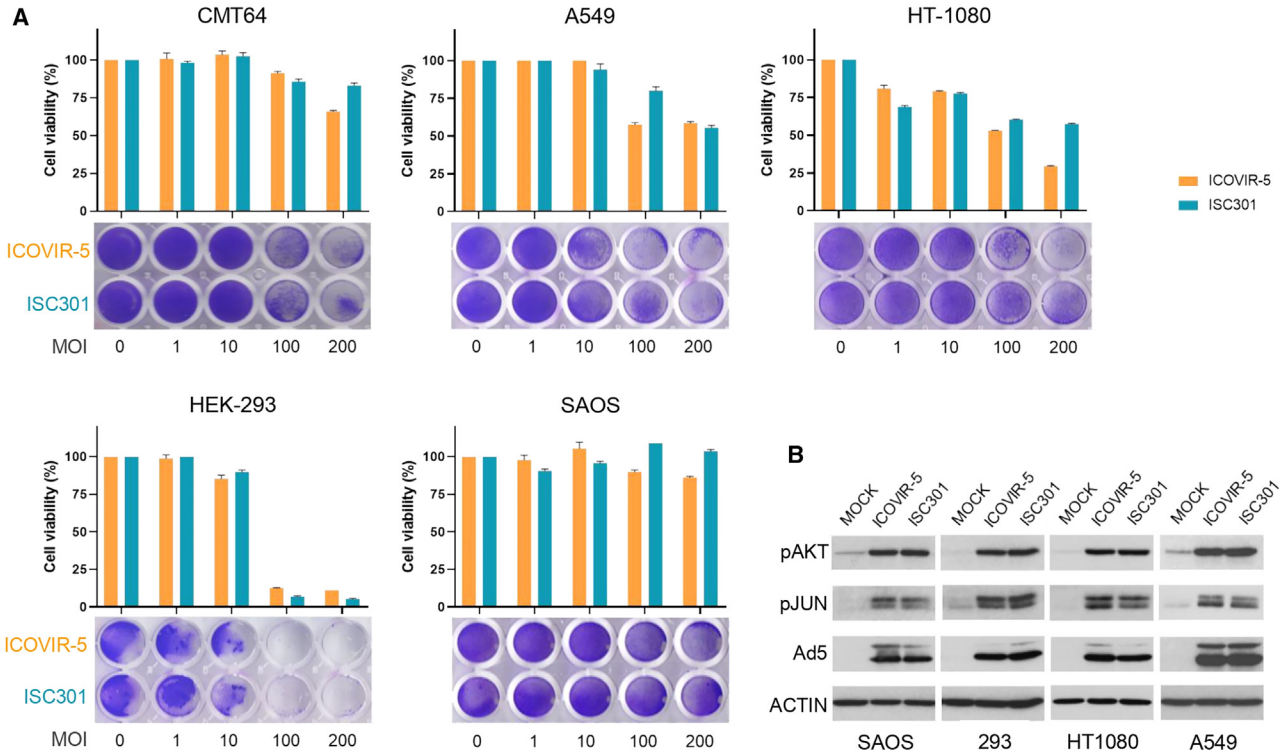

Figure 2. Effect of ISC301 infection on cell viability and signaling pathways

(A) Visualization and semi-quantification of cells infected with ICOVIR-5 and ISC301 at the indicated MOIs for 72 h (SAOS-2, HEK-293, A549, and CMT64) or 96 h (HT-1080), stained with crystal violet to detect cell viability. Bar graphs represent mean + SD. (B) Phosphorylation of AKT and cJUN 24 h after infection with ICOVIR-5 and ISC301 (MOI = 2) was studied by western blot in the human cell lines. Expression of Ad5 (adenovirus expression control) and actin (loading control) are also shown.

penton base of oncolytic virus—while maintaining the artificial RGD domain in the fibers—improves the antitumor potency of adoptive cellular immunotherapies.

RESULTS

Generation of a penton base RGD-motif deleted oncolytic adenovirus

Most human adenoviruses possess an RGD domain at the penton base, while CAVs do not possess this integrin-binding domain. On the other hand, the OAds ICOVIR5 and ICOCAV17 have been modified to express these RGD domains in the H1 loop of the fiber knobs. Based on previous clinical results, we hypothesized that the absence of the penton base RGD motifs in ICOCAV17 might be related to the better clinical outcomes of canine Celyvir. Accordingly, we engineered a novel human OAd, which we named ISC301, based on ICOVIR-5 in which the penton base RGD motifs were mutated (Figure 1A). So, changes in three nucleotides of the penton base resulted in the change of the RGD motif to the amino acid sequence Arg-Ala-Glu (RAE) (Figure 1B), a classical non-binding integrin motif,[21] but still maintaining RGD motifs in the fiber knobs.

ISC301 production in HEK293 cells and further CsCl gradient purification resulted in higher proportion of empty capsids than ICOVIR-5 (Figure S1A). Production of ISC301 in human HEK293 cells was analyzed through western blotting, revealing comparable protein profiles despite a slight decrease in adenoviral protein expression in ISC301-infected cells (Figure 1C). No differences in production were observed in the semi-permissive murine cell line CMT64, commonly utilized in immunocompetent models for virotherapy (Figure S1B). These results align with the observation that F-type human adenoviruses are difficult to grow *in vitro*.[24] Furthermore, the deletion of the penton base RGD motif impaired the ability of adenoviruses to escape from endosomes, leading to a modified pattern of intracellular trafficking and delayed delivery of viral particles to the nucleus.[21] Purified ICOVIR-5 and ISC301 complete capsids were observed using transmission electron microscopy (TEM) (Figure 1D).

ISC301 and ICOVIR-5 induce similar *in vitro* cytotoxic effect in tumor cell lines

Oncolytic effect of ISC301 was studied *in vitro* and compared with ICOVIR-5. We assayed cell survival *in vitro* after OAd infection of human tumor cell lines A549, HT-1080, SAOS-2, and HEK293, and the semi-permissive murine cell line CMT64 (Figure 2A). Cell viability after infection with ICOVIR-5 and ISC301 at different multiplicities of infection (MOI = 0, 1, 10, 100, and 200 PFU/cell) was

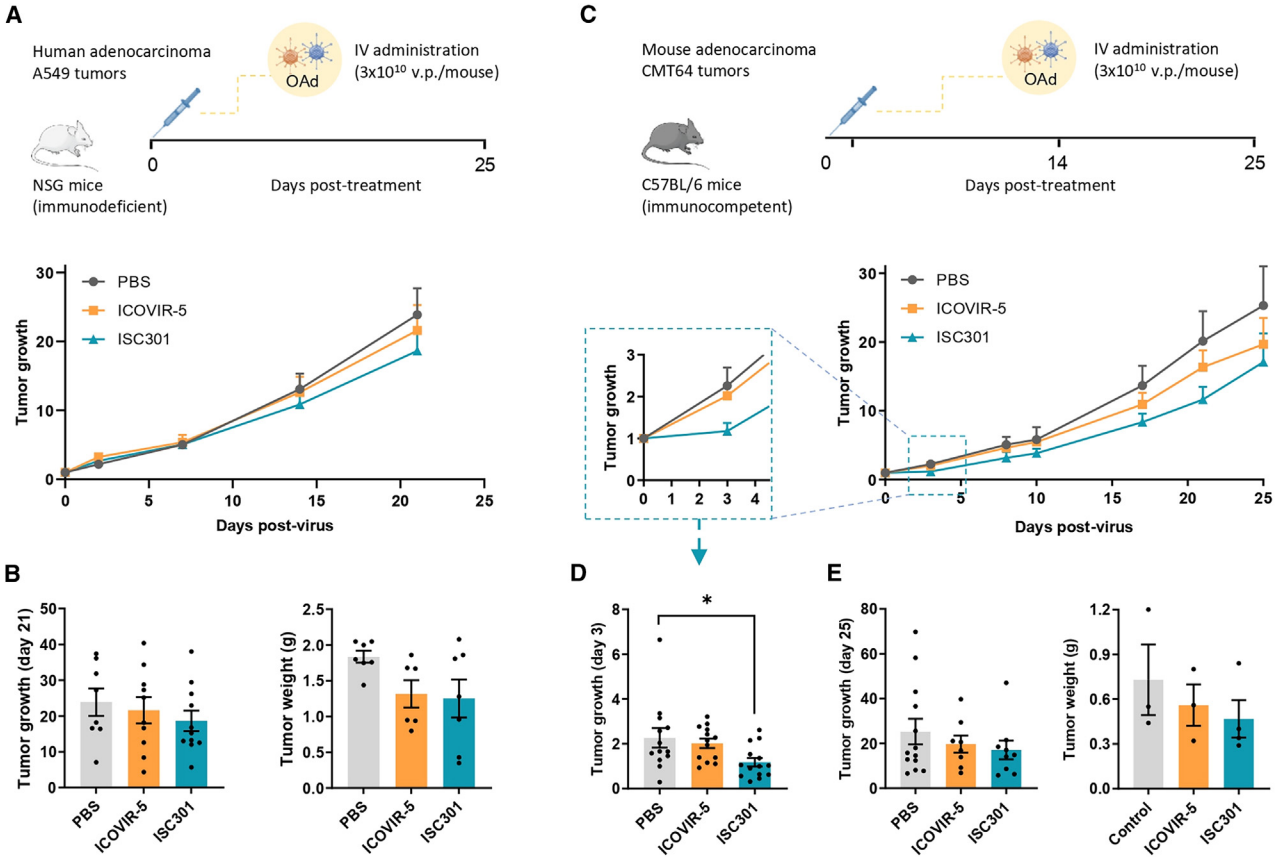

Figure 3. *In vivo* antitumor efficacy of ISC301 is significant at early days

(A) Schematic illustration of *in vivo* experimental design and follow-up of tumor growth in immunodeficient (NSG) mice treated with PBS (gray), ICOVIR-5 (yellow), or ISC301 (blue) represented as mean +SEM (n = 8). (B) Tumor growth and tumor weight of immunodeficient mice treated with PBS, ICOVIR-5, or ISC301 at endpoint (day 21). (C) Schematic illustration of *in vivo* experimental design and follow-up of tumor growth in immunocompetent (C57BL/6) mice treated with PBS, ICOVIR-5, or ISC301 represented as mean +SEM. (D) Tumor growth of C57BL/6 mice treated with PBS, ICOVIR-5, or ISC301 at day 3 (n = 8–13). (E) Tumor growth (n = 8–13) and tumor weight (n = 3) at endpoint (day 25). Bar graphs represent mean ± SEM. One-way ANOVA followed by Tukey's multiple comparisons test. *$p < 0.05$.

assessed by staining attached cells with crystal violet at various times post-infection. Overall, we did not detect relevant differences on *in vitro* infectivity in all cells tested, although a lower cytopathic effect of ISC301 seemed to be observed on HT-1080 (MOI = 200). HEK293 cells displayed similar sensitivity to both OAds, as no cells remained attached at MOI of 100 or higher 72 h post-infection. Finally, SAOS-2 cells were much less susceptible to ICOVIR-5- and ISC301-mediated cytotoxicity and little cytopathic effect was detected in both cases.

ISC301 and ICOVIR-5 induce similar signaling after infection of tumor cell lines

We also studied the effect of OAd infection in the activation of AKT and cJUN signaling pathways (Figure 2B). Western blot analysis showed that ICOVIR-5 and ISC301 induced AKT and cJUN phosphorylation at similar levels in all human lines. Protein profiles using antibodies directed against Ad5 proteins were also comparable in all lines (Figure 2B).

ISC301 and ICOVIR-5 show similar *in vivo* antitumor effect

The *in vivo* antitumor efficacy of ICOVIR-5 and ISC301 was compared *in vivo* in an immunodeficient mouse model of NSG mice bearing human adenocarcinoma tumors. After 3 weeks of treatment, intravenous administration of a single dose of ISC301 showed similar results to using the OAd ICOVIR-5 (Figures 3A and 3B).

We therefore studied the antitumor efficacy of ISC301 in an immunocompetent mouse model previously developed by our group. The tumor was modeled using CMT64, a mouse adenocarcinoma cell line that is semi-permissive to ICOVIR-5 replication (Figure 3C).[25,26] Three days after administration of a single dose, mice treated with ISC301 showed significant lower tumor growth than those treated with ICOVIR-5 or a control group (Figure 3D). A similar tendency was observed during the follow-up, showing lower tumor growth than using ICOVIR-5 or—especially—the control group, although no significant differences were observed (Figures 3C–3E).

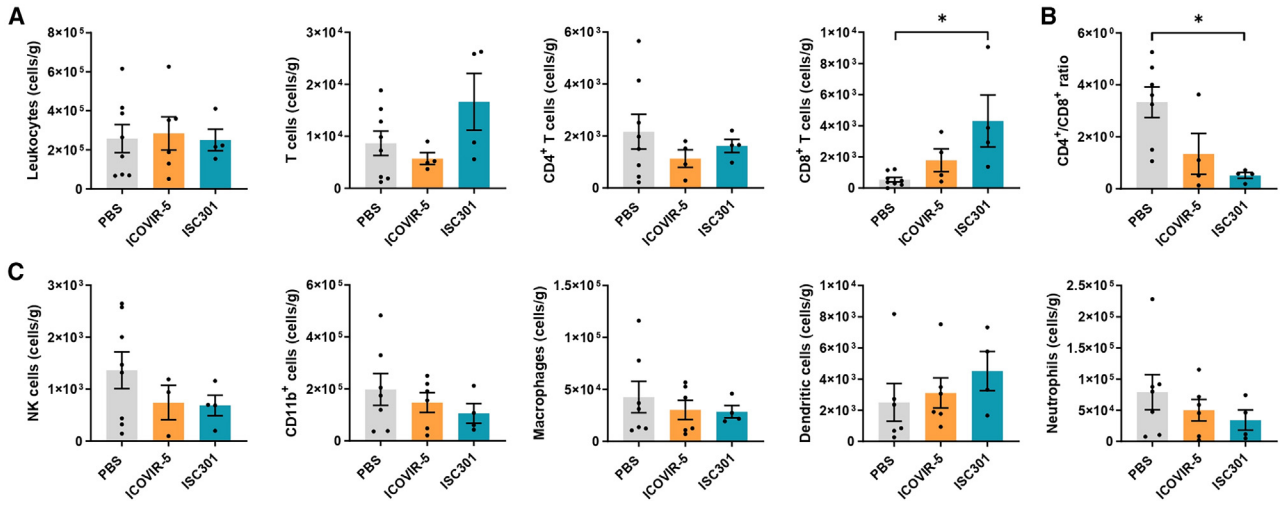

Figure 4. ISC301 increases tumor infiltration of CD8⁺ T cells

(A) Density of tumor-infiltrating leukocytes, total T cells, CD4⁺ T cells, and CD8⁺ T cells in resected CMT64 tumors at endpoint, expressed as cells per gram of tumor, in mice treated with PBS, ICOVIR-5, or ISC301 ($n = 4–8$). (B) CD4⁺/CD8⁺ ratio. (C) Density of tumor-infiltrating innate immune populations and NK cells. Bar graphs represent mean ± SEM. One-way ANOVA followed by Tukey's multiple comparisons test. *$p < 0.05$.

ISC301 increases tumor infiltration of CD8⁺ T cells and decreases CD4⁺/CD8⁺ T cell ratio

Considering the potential role of the immune system on OAd-mediated antitumor effects, we analyzed tumor-infiltrating immune cells by flow cytometry in the immunocompetent model treated with ISC301. Although density of leukocytes was similar in the control group and groups treated with the OAds, a slight increase of tumor-infiltrating T cells was observed in those treated with ISC301 compared with ICOVIR-5 or PBS (Figure 4A). Previous results showed that oncolytic virotherapy using ICOVIR-5 seems to induce higher infiltration of CD8⁺ T cells.[27] Here, we observed that ISC301 induced even higher infiltration of CD8⁺ T cells than ICOVIR-5, significant in comparison with the control group. As a result, the CD4⁺/CD8⁺ ratio, previously shown to decrease after treatment with ICOVIR-5, was significantly reduced in tumors treated with ISC301 compared with those treated with PBS (Figure 4B). Study of innate immune populations at endpoint did not show significant differences in tumors treated with PBS, ICOVIR-5, or ISC301 (Figure 4C).

ISC301 induces higher pro-inflammatory response in peripheral blood than ICOVIR-5

Previous results in our laboratory have demonstrated the relevance of the systemic pro-inflammatory status after administration and delivery of oncolytic virotherapy.[27] We therefore performed a complete analysis of peripheral blood from tumor-bearing mice treated intravenously with ICOVIR-5 and ISC301 (Figure 5A). Forty-eight hours after treatment, mice treated with either ISC301 or ICOVIR-5 showed significant decrease of leukocytes and lymphocytes than the control group (Figures 5B and S2). Biochemical parameters were analyzed, and no major differences were observed between the PBS, ISC301, and ICOVIR-5 samples (Figure 5C), demonstrating a safe biochemical profile following intravenous administration of both OAds. Only glutamic-pyruvic transaminase levels were higher in mice treated with ICOVIR-5 compared with the control group, whereas no significant differences were observed in the ISC301 group (Figure 5C), reinforcing its safe profile.

We also used an array of 40 cytokines to analyze mice peripheral blood 48 h after the single dose of OAds. The results showed distinct profiles of pro-inflammatory cytokines between the two OAds. Specifically, ISC301 administration induced higher expression levels of CXCL1, CXCL12, CCL2, and IL-16 compared with ICOVIR-5 or PBS (Figure 5D). Interestingly, this heightened pro-inflammatory profile after ISC301 administration readjusted by 11 days post-treatment, showing similar results between both OAd administrations, akin to the control group (Figure S3).

ISC301 induces early activation of the NF-κB pathway in the tumor

NF-κB induces the expression of pro-inflammatory genes, including those encoding interferon, cytokines and chemokines, so we analyzed OAd-induced activation of the NF-κB pathway *in vitro* and *in vivo*. CMT64-6 cells harboring a reporter luciferase construct under the NF-κB promoter (CMT64-NF-κB-luc) were infected *in vitro* with ICOVIR-5 or ISC301 and luciferase expression was monitored during 72 h (Figure 6A). Luciferase activity showed a similar pattern in both OAd groups, with increasing expression at 24 h post-infection, although even significant higher levels were detected in ISC301-infected cells compared with those infected with ICOVIR-5 (Figures 6B and 6C).

Next, CMT64-NF-κB-luc tumor cells were inoculated subcutaneously in C57BL/6 mice to study this parameter *in vivo*. Mice were

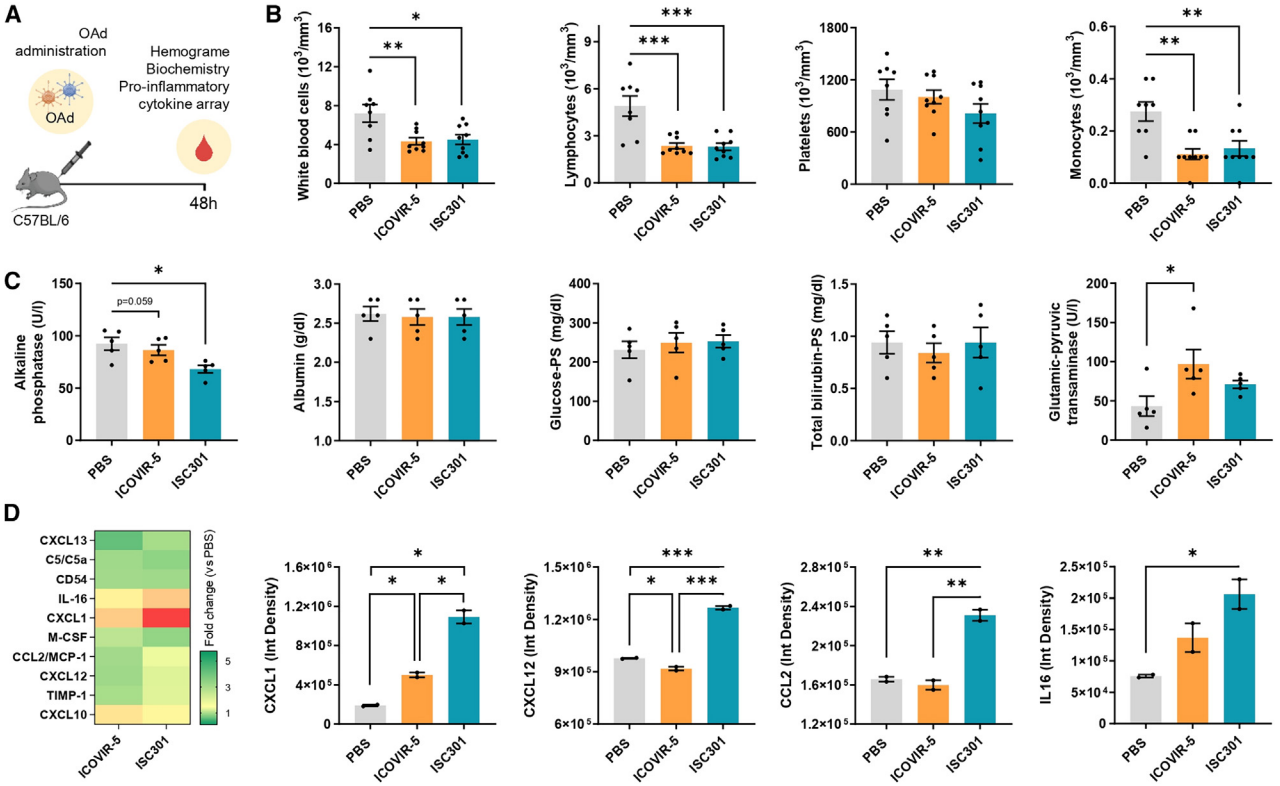

Figure 5. ISC301 induces higher pro-inflammatory response in peripheral blood than ICOVIR-5

(A) Immunocompetent C57BL/6 mice were i.v. inoculated with the OAds ICOVIR-5 or ISC301. (B) Analysis of peripheral blood cell populations (n = 8–9). (C) Biochemical analysis of peripheral blood at 48 h after OAd administration (n = 4). (D) Cytokine detection in peripheral blood at 48 h after OAd administration (n = 2–3). On the left, heatmap showing fold change in comparison with the PBS control group (lower expression in green, higher expression in red). On the right, cytokine detection measured by intensity of density. Bar graphs represent mean ± SEM. One-way ANOVA followed by Tukey's multiple comparisons test. *p < 0.05, **p < 0.01, ***p < 0.001.

intravenously inoculated with ICOVIR-5 or ISC301 and NF-κB activation was monitored in the tumors by *in vivo* luciferase activity for 6 days (Figure 6D). Only 6 h after virus administration, tumors from mice treated with ISC301 presented significant higher activation of the NF-κB pathway than those treated with ICOVIR-5 or PBS (Figures 6E and 6F). This difference was also observed at 24 h and maintained until 6 days post-treatment (Figures 6E and 6F). In conclusion, ISC301 induces inflammation in the tumor microenvironment earlier than ICOVIR-5.

ISC301 improves antitumor efficacy of CAR T cell therapy

It is well known that hot solid tumors show better response to immunotherapies. As our previous results showed that ISC301 induces high pro-inflammatory response in the tumor microenvironment at short times after intravenous administration, we consider its combination with other immunotherapies, such as CAR T cells.

First, appropriate NKG2D CAR T characterization was assessed (Figures 7A–7C). Then, the potential synergy of the OAds and CAR T cell therapy was studied *in vitro*. Tumor cell viability after 72 h of infection with ICOVIR-5 and ISC301 at 2 PFU/cell and 24 h of CAR T coculture was assessed by flow cytometry (Figure 7D). Overall, we detected significant differences in the *in vitro* combination therapy compared with infected cells, although no significant differences were observed between viruses.

As we have previously observed differences in the results obtained *in vitro* and *in vivo*, we also performed an *in vivo* study of the combination (Figure 7E). Human A549 tumors were implanted in NSG mice, and once the tumors reached a measurable size, the animals were administered a single intravenous dose of either ISC301 or ICOVIR-5. Given our previous observation of CAR T cells exhibiting tumor homing within the initial 24 h,[28] we decided to administer CAR T cells intravenously 1 day after the administration of OAd (Figure 7E). Interestingly, while mice treated with CAR T cell therapy showed some antitumor efficacy, combination with ISC301 enhanced the antitumor potency of the immunotherapy (Figures 7E–7H). As a result, combination of ISC301 and CAR T cells showed significant antitumor efficacy during the follow-up compared with the PBS group (Figures 7G and 7H).

DISCUSSION

Anticancer immunotherapies have emerged as new therapeutic approaches within oncology. These treatments focus on overcoming

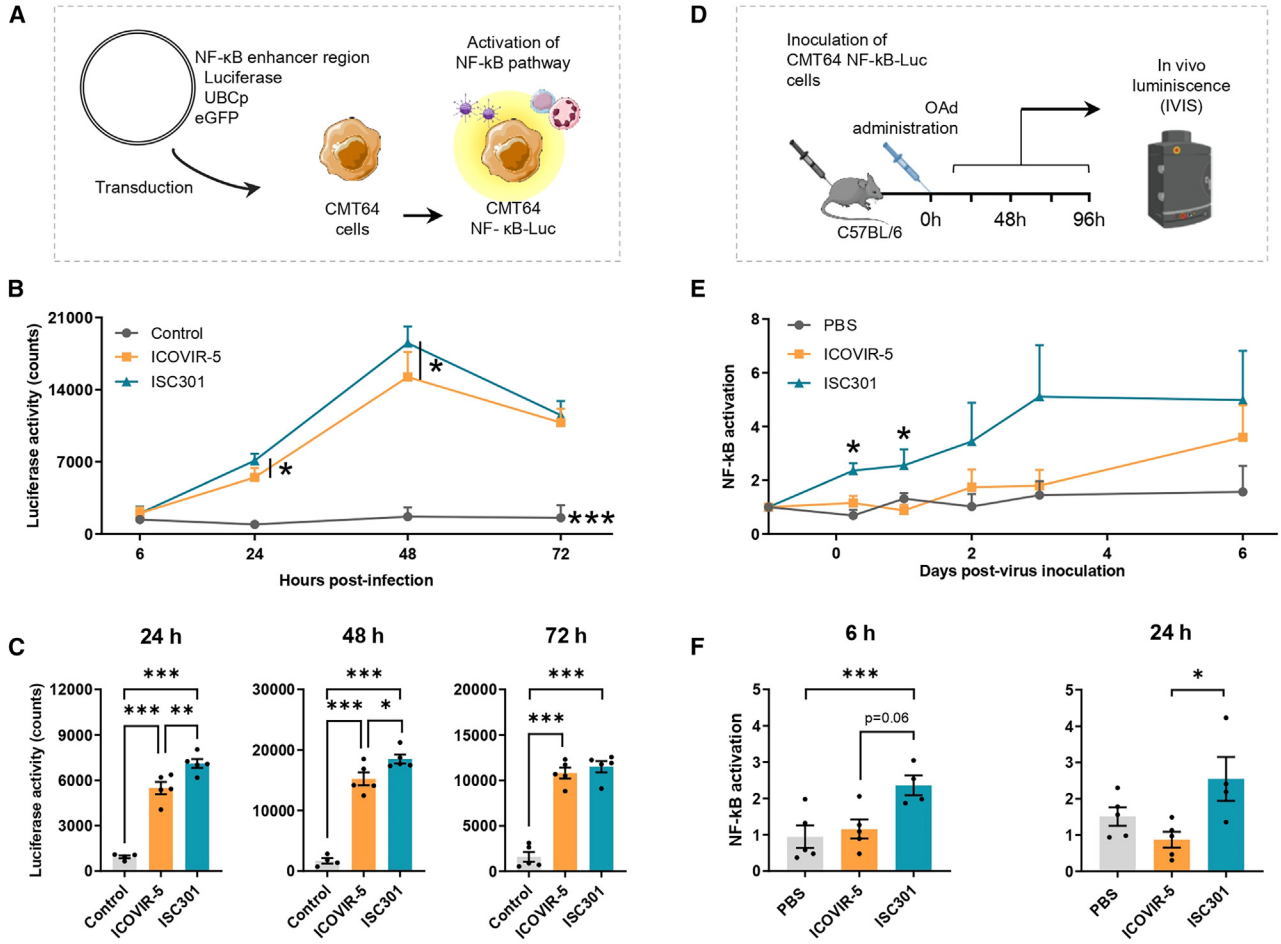

Figure 6. *In vitro* and *in vivo* activation of NF-κB in the tumor

(A) CMT64 were transduced with a vector expressing luciferase under NF-κB responder-promoter, obtaining CMT64- NF-κB-Luciferase tumor cells. (B) Kinetic of *in vitro* NF-κB activation detected by luciferase activity in CMT64 cells after OAd infection. Mean + SD. (C) NF-κB activation detected by luciferase activity in CMT64 cells at 24, 48, and 72 h after OAd infection ($n = 5$). Mean ± SD. (D) CMT64- NF-κB-Luciferase tumor cells were inoculated in C57BL/6 mice, so *in vivo* activation of the NF-κB pathway is detected by luminescence. (E) NF-κB activation *in vivo* was monitored during 6 days. Mean + SEM (F) *In vivo* NF-κB activation detected by luciferase activity after OAd administration, tumors treated with ISC301 presented higher activation of NF-κB than those treated with PBS or ICOVIR-5. This tendency was also observed at 24 h ($n = 5$). Mean ± SEM. One-way ANOVA followed by Tukey's multiple comparisons test. $^{*}p < 0.05$, $^{**}p < 0.01$, $^{***}p < 0.001$.

tumor-induced immunosuppression and the resulting activation of immune subpopulations. Multiple efforts are being generated in treatments based on cytokines, vaccines, adoptive cell therapies, oncolytic viruses, and antibodies against immune checkpoint inhibitors. Combinations of immunotherapies have also been proposed, especially with oncolytic viruses because of their ability to inflame tumors which then would be more susceptible to other immunotherapies, such as checkpoint inhibitors or adoptive cellular therapies.

Talimogene laherparepvec (Imlygic) was the first oncolytic virus approved by the FDA and EMA for the local treatment of melanomas. The mechanisms of action of Talimogene laherparepvec include the direct lysis of tumor cells (stimulating a local response in the tumor microenvironment) and a concurrent systemic immune response powered by secretion of the granulocyte-macrophage colony-stimulating factor.[29] Similarly, Teserpaturev, another HSV-based oncolytic virus approved in Japan, also increases the tumor-infiltrating $CD4^{+}$ and $CD8^{+}$ lymphocyte populations in glioblastomas.[30] On the other hand, OAds were the first oncolytic virus to be used in the clinic, with ONYX-015 (Oncorine) being approved in 2005 for the treatment of head and neck cancers in China.[31] Nowadays, OAds are the oncolytic viruses most commonly used in clinical trials,[32] many of which contain extra RGD motifs in the fibers.[33,34] In this sense, the replacement of an RGD sequence by an RAE mutation, as we describe here, in their penton base might improve the immune activation of these OAds, especially if they are used in combination with other immunotherapies.

Although ISC301 is viable, a higher number of empty capsids was obtained in independent productions in HEK293 cells. The crystal

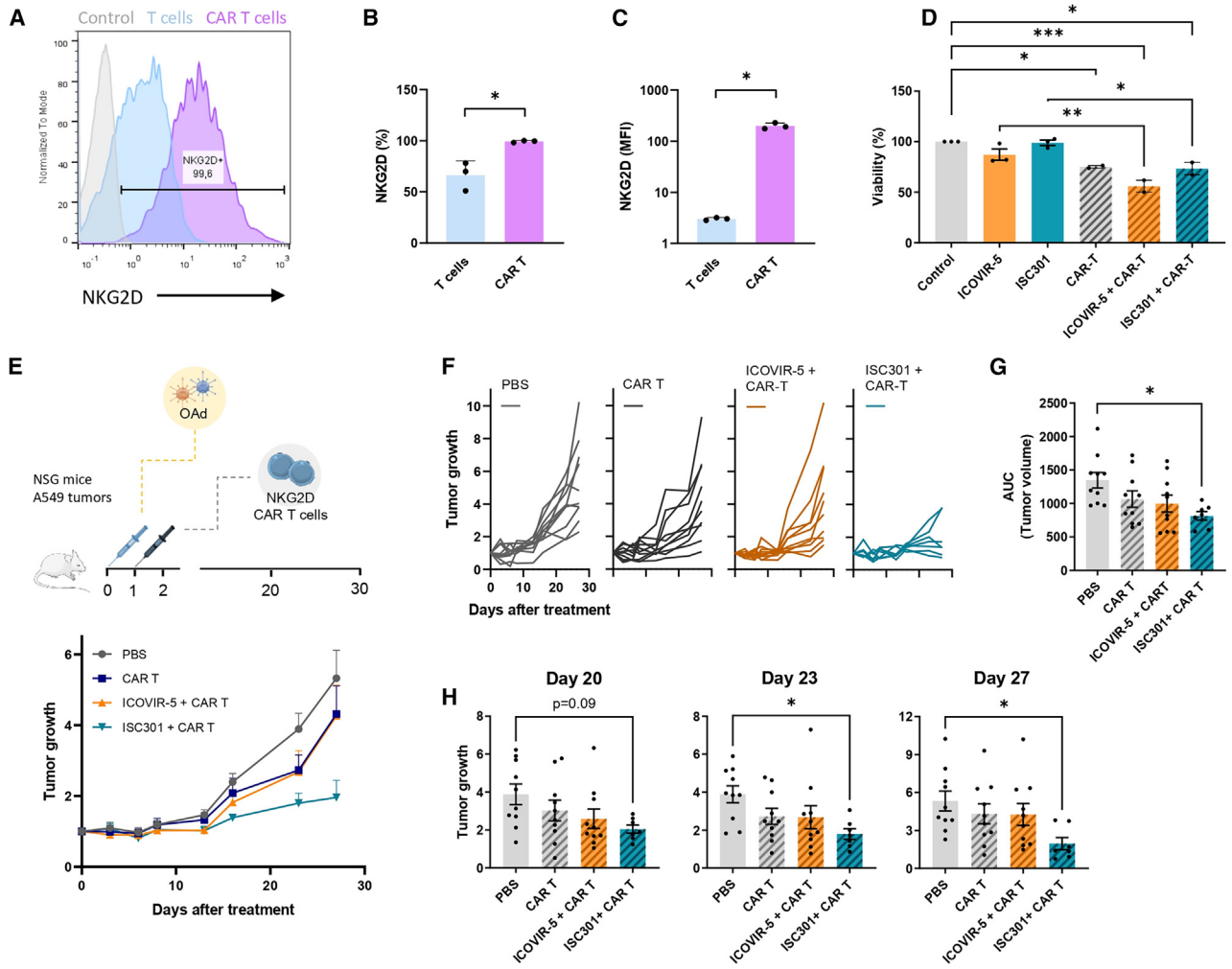

Figure 7. ISC301 improves antitumor efficacy of CAR T cell therapy

(A) Histogram showing expression of NKG2D on non-transduced T cells (control, gray), T cells (blue), and NKG2D CAR T cells (purple). (B and C) Mean fluorescence intensity (B) and percentage of expression (C) of NKG2D on CAR T cells ($n = 3$). Mean + SD. Parametric t test. (D) *In vitro* tumoral cell viability after 72 h of infection with ICOVIR-5 and ISC301 and 24 h of NKG2D CAR T coculture. (E and F) At the top (E), schematic illustration of *in vivo* experimental design. Immunodeficient NSG bearing subcutaneous A549 tumors were treated intratumorally with OAd ICOVIR-5 or ISC301, followed by intravenous administration of NKG2D CAR T cells 24 h later. At the bottom (E), follow-up of tumor growth in mice treated with PBS (gray), NKG2D CAR T cells (dark blue) or combination of NKG2D CAR T with ICOVIR-5 (yellow) or ISC301 (blue) represented as (E) mean +SEM, and (F) individual values ($n = 7–10$). (G) Areas under the curve (AUC) of treated mice ($n = 7–10$). (H) Tumor growth of treated groups at indicated days. Bar graphs represent mean ± SEM. One-way ANOVA followed by Tukey's multiple comparisons tests. $^{*}p < 0.05$, $^{**}p < 0.01$, $^{***}p < 0.001$.

structure of the human Ad2 penton base has shown that the RGD motif, required for interactions with cellular integrins, occurs on a hypervariable flexible loop exposed on the capsid surface.[35] Despite the change of the RGD sequence in the penton base of ISC301, we have not observed a significant reduction in infectivity capacity. In this context, previous studies showed that penton base RGD motif deletion did not affect attachment to A549 cells but resulted in slower internalization into cells.[21] Similarly, penton base RGD motifs are required for efficient transduction and activation of endothelial cells using adenovirus vectors.[36] However, it has been shown that incorporation of an RGD-containing peptide in the HI loop of the adenovirus fiber knob domain allows the adenovirus to utilize RGD-integrin interactions as an alternative infection pathway, improving the ability of the adenovirus to transduce or infect several types of cells.[37] Thus, ISC301 might interact with CAR and also integrins, through their RGD motifs in the fiber knob, which may explain why we did not find differences in infection tropism between ISC301 and ICOVIR-5.

A key component of the host innate immune response to adenovirus involves the expression of pro-inflammatory cytokines regulated by NF-κB.[38] During viral infections, AKT is recognized for positively regulating NF-κB.[39,40] Following adenoviral infection, NF-κB activation seems to occur in waves, presumably inducing distinct patterns of gene expression throughout the course of an acute infection.[41]

The initial wave is controlled by a swift and transient activation mediated by PI3K/Akt signaling, which is triggered by the interaction between adenoviral capsids and alpha(v) integrin receptors in epithelial cells.[42] A second wave has been linked to Toll-like receptor (TLR)-dependent and -independent pathways in a cell-type-specific fashion.[43] We observed no differences in the activation of AKT or c-JUN pathways in ISC301 infection compared with ICOVIR-5. However, previous studies in kidney epithelium-derived cells following transduction with a penton base RGD-deleted vector showed no activation of AKT, confirming the importance of capsid-alpha(v) integrin interactions in adenovirus-induced AKT activation.[42] Thus, the precise mechanism through which ISC301 activates AKT phosphorylation is unknown, although it is possible that the interaction with integrins of the RGD motif on the fiber activates AKT similarly to what has been described for the RGD sequences on the penton base. Similarly, mouse adenovirus type 1 lacks an RGD sequence in the virion penton base protein, but has a natural RGD sequence in the fiber knob that interacts with alpha(v) integrin serving as a primary receptor.[44] This alternative activation by the RGD motif in the fibers could explain that the activation of the NF-κB pathway *in vitro* seems to be identical in both OAds. However, the differences observed *in vivo* could be due to other mechanisms.

Some adenovirus species (D and B) tend to accumulate in late endosomes following cellular entry rather than experiencing early endosomal escape adenovirus species C, as Ad5 do. This accumulation in late endosomes can trigger higher antiviral innate immune responses through interactions with sensors such as TLRs.[45] Indeed, immunization with adenovirus species D and B induces greater levels of innate cytokine responses compared with adenovirus serotype 5 in rhesus monkeys.[46] As effective viral escape from endosomes depends on RGD-penton base interactions with cellular integrins,[21] it could be hypothesized that ISC301 would experience this rapid escape less efficiently and may also accumulate within late endosomes, behaving like adenoviruses of species D and B and leading to a rapid and enhanced NF-κB activation, ultimately resulting in elevated intratumoral inflammation.

Upon adenovirus entering the bloodstream, multiple components within the blood attach to the capsid. These blood elements effectively bind to viral particles, leading to interactions between the virus-blood factor complexes and a distinct array of receptors, thus allowing these complexes to enter cells using mechanisms that are not accessible to the "naked" virus.[47] In this context, α-defensins bind human adenovirus and prevent virus uncoating and release of the endosomalytic protein VI during cell entry. The adenoviral binding sites for α-defensins are located in the interface of the penton base and fiber.[48] So, it is possible that α-defensins bind ISC301 with higher affinity than ICOVIR-5 and it has been described that defensin-stabilized OAds reach the late endosome at higher frequency, stimulating a more potent NF-κB response in our *in vivo* model.[49]

On the other hand, it has been described that the Ad5 penton base RGD motif mediated interactions with liver endothelial cells and hepatocytes, inducing virus retention.[50] An RGD motif deleted OAd as ISC301 would overcome this physiological obstacle and infect the tumor in greater quantity and at a faster rate, leading to a rapid increase in NF-κB activation.

Combinations of OVs with alternative immunotherapies have led to promising progress in cancer treatment. The induction of systemic innate and tumor-specific adaptive immune responses seems to constitute a crucial component in achieving tumor elimination through oncolytic viruses. The adenoviral infection triggers a pro-inflammatory response with a defined set of cytokines and chemokines leading to an immune activation.[47] In tumoral cells, OAds also induced autophagy and immunogenic cell death enhancing innate immune response.[47] In our immunocompetent mice model, using ISC301 and ICOVIR-5, we also detected an increase in tumors of subpopulations of immune infiltration cells being higher in TILs when we used ISC301. Moreover, our data indicated a lower $CD4^+/CD8^+$ ratio in intratumoral TILs when mice were treated with ISC301 compared with ICOVIR-5 and non-treated controls. These results are in agreement with a higher inflammation of tumor, with an increase of systemic pro-inflammatory cytokines, which induces a higher immune subpopulation infiltration into the tumor and a better balance of these subpopulations; indicating an improved capacity of ISC301 in the antitumoral activation of the immune system. In this line, higher $CD8^+$ T cell infiltration has been associated with a better response to immunotherapy, such as CAR T cell therapy.[51] These properties of OAds, together with the induced inflammatory profile, could be used to overcome obstacles of antitumoral adoptive cell therapies, such as CAR T cells, including limited tumor infiltration of CAR T cells and the presence of an immunosuppressive tumor microenvironment.[52]

We are working in the clinical field with the NKG2D CAR T cell therapy. This design specifically targets NKG2D ligands and is currently under evaluation in a phase I clinical trial (EudraCT number 2019-004310-33; CAR4SAR). NKG2D receptors are overexpressed in certain tumors,[53] and the ligands for the NK activating receptor NKG2D are upregulated in cells upon adenoviral infection.[54] While the combination of OAds and CAR T in our *in vitro* experiments—conducted under suboptimal conditions—did not demonstrate a synergistic effect, noteworthy findings emerged from our *in vivo* experiments. Specifically, enhanced antitumor efficacy was observed when ISC301 and CAR T cells were combined, surpassing the outcomes of other experimental groups. The heightened pro-inflammatory activity induced by ISC301 in the initial hours following administration would likely promote the homing and intratumoral activation of CAR T cells. Consistent with this notion, our previous results indicated that CAR T cell homing in this murine model occurred within the first 24 h.[28] Therefore, the enhancement in antitumor activity is likely attributable to the increased tumor inflammation induced by ISC301, facilitating the homing and activation of the administered CAR T cells. Indeed, studies have highlighted a synergistic effect between CAR T cells and non-CAR immune cells in combating tumors.[55] This

synergy suggests that the co-presence of $CD8^+$ T cells—as we observed in ISC301-treated tumors—alongside CAR T cells may amplify the overall antitumor response. In addition, recent findings suggest that the effectiveness of immunotherapies may vary with the time of day due to the endogenous circadian clock of leukocytes and rhythmic leukocyte infiltration.[56] Furthermore, the efficacy of CAR T cell therapy can be enhanced by adjusting treatment timing accordingly.[56] In our study, mice were treated in the morning; however, optimizing the timing of treatment could potentially improve outcomes.

The strategy of combining OAds and CAR T has already entered human clinical trials,[57] making this immunotherapy combination a highly active field in coming years. In the foreseeable future, this combination could be considered as the next step in our phase I clinical trial of NKG2D CAR T cells for the treatment of sarcoma in children, adolescents, and young adults. In addition, the development of oncolytic virotherapy based on adenoviruses has made significant progress in recent years, with 20 different genetically engineered versions of these vectors recently being used in more than 42 clinical trials.[33] The modification in the penton base RGD sequence of the OAd ISC301 could be integrated into the extensive array of OAds being tested in preclinical models and these clinical trials.

MATERIALS AND METHODS

Cell culture

Human cell lines A549, HT-1080, HEK293, and SAOS-2 and murine CMT64-6 were cultured in Dulbecco's modified Eagle's medium (DMEM) supplemented with heat-inactivated 10% fetal bovine serum (FBS), 2 mM glutamine, streptomycin (100 mg/mL), and penicillin (100 U/mL) (complete DMEM). All cell lines were routinely cultured under standard conditions (a humidified atmosphere with 5% CO_2, 37°C) in their appropriate medium. All culture reagents were obtained from Lonza Bioscience except for FBS, which was purchased from Sigma-Aldrich (Science Exchange, RRID: SCR_010620; St. Louis, MI).

Adenoviruses

ICOVIR-5 has been extensively described elsewhere.[8] In brief, ICOVIR-5 (Ad-DM-E2F-K-Δ24RGD) is an optimized human OAd that combines E1a transcriptional control by an insulated form of the E2F promoter with the Δ24 mutation of E1a to improve the therapeutic index of AdΔ24RGD. ICOVIR-5 also contains the Kozak sequence at the E1a start codon, which is important to restore E1a expression and viral replication to AdwtRGD levels in tumor cells. It also incorporates an RGD motif in the H1 loops of the fiber knobs. ISC301 was derived from ICOVIR-5 and was constructed by homologous recombination in yeast of FseI-digested pICOVIR-5 with a DNA fragment of a plasmid that contained a penton base sequence with a mutated RGD motif. Specifically, three nucleotides of the penton base were modified, changing the RGD motif of the penton base to the amino acid sequence Arg-Ala-Glu (RAE). Mutations were confirmed by PCR amplification of the region and sequencing both strands of the PCR product. DNA sequencing was carried out in the facilities of the Servicio de Genómica at Instituto de Salud Carlos III (Madrid, Spain) using the ABI DNA Analyzer 3730xl (Applied Biosystems, Foster City, CA). Construction of ΔP-L2 adenoviral vector was described previously.[58] Both adenoviruses were generated by the transfection of PacI-linearized plasmid into HEK293 cells and purified by CsCl gradient centrifugation.

TEM

For negative staining, small aliquots of adenovirus suspension were adsorbed for 5 min onto glow-discharged 300 mesh carbon-coated collodion microscopy copper grids, negatively stained with 2% (w/v) uranyl acetate, and air-dried. The samples were then analyzed on an FEI Tecnai-12 electron microscope equipped with a LaB6 filament operated at 120 kV. Images were recorded at nominal magnifications on a CCD (charged-coupled device) FEI Ceta digital camera.

Western blot analysis

Total proteins were extracted with SDS sample buffer (62.5 mM Tris [pH 6.8], 2% SDS, 10% glycerol, 1 mM phenylmethylsulfonyl fluoride, 5 mM NaF, 20 mM β-glycerophosphate, 0.1 mM Na_3VO_4, and 1:100 protease inhibitor cocktail from Sigma-Aldrich). Then, samples were boiled at 95°C for 5 min and sonicated (three pulses of 30 s on ice). Protein concentrations were determined using the DC Protein Assay (Bio-Rad Laboratories, RRID: SCR_008426, Hercules, CA). Finally, DTT and bromophenol blue were added to the samples to a final concentration of 100 mM and 0.1%, respectively, and then boiled at 95°C for 5 min. Proteins were separated by 10% SDS-PAGE and blotted on PVDF membranes (Bio-Rad Laboratories). Primary antibodies were rabbit polyclonal anti-Ad type 5 1:20,000 dilution (Abcam), mouse monoclonal anti-c-Jun (phospho S63) 1:1,000 dilution (Santa Cruz Biotechnology), rabbit monoclonal anti-AKT1 (phospho S473), 1:1,000 dilution (Epitomics), and mouse monoclonal anti-β-actin, 1:100,000 dilution (Sigma-Aldrich). Secondary antibodies were polyclonal goat anti-rabbit and anti-mouse immunoglobulins/HRP, 1:3,000 dilution (Agilents Dako, Agilent, cat. no. P0447, RRID: AB_2617137; Santa Clara, CA). Signal was detected using the Immobilon Western Chemiluminescent HRP Substrate (Merck Millipore, Madrid, Spain).

Phosphokinase array analysis

Phosphorylation profiles after adenoviral infection was analyzed using the Proteome Profiler Human Phospho-Kinase Array (R&D Systems, Minneapolis, MN) according to the manufacturer's instructions. The array detects phosphorylation of 43 human kinases and total amounts of 2 related proteins. Cell lysates (400 μg) from either control or adenovirus-infected samples were incubated with each set of nitrocellulose membranes of the array with the spotted capture antibodies. Array images were scanned, digitized, and the pixel density of the spots was quantified using ImageJ software (RRID: SCR_003070). The average density of duplicated spots representing each protein was used to determine changes in phosphorylated proteins or cytokines.

Cytotoxicity assay

To analyze the toxic effects of ICOVIR-5 and ISC301, 5×10^4 cells were seeded on 48-well plates. After 24 h, cells were infected for 2 h

in serum-free DMEM with each virus at various MOIs, washed with PBS, and incubated in complete DMEM for 48 and 72 h. For staining of attached cells, medium was removed, cells were washed with PBS, fixed with 10% formaldehyde for 10 min, stained with 0.2% crystal violet for 10 min, and rinsed with water. Air-dried dishes were photographed. The experiments were repeated three times.

Animal studies

For *in vivo* antitumor experiments in an immunodeficient model, 5×10^6 A549 tumor cells were implanted subcutaneously in 7-week-old NSG mice. For an *in vivo* immunocompetent model, 1×10^6 CMT64 tumor cells were implanted subcutaneously in 7-week-old C57BL/6 mice. When the tumors were measurable, PBS, ICOVIR-5, or ISC301 were inoculated intravenously (3×10^{10} vp/mouse in a total volume of 100 mL). In experiments studying the combination of immunotherapies, PBS or NKG2D CAR T cells were administered intravenously (5×10^6 cells/mouse in a total volume of 100 mL) 1 day after OAd administration (3×10^{10} vp/mouse). Tumor length (L), width (W), and height (H) were measured with a caliper periodically and tumor volume was calculated as $(L \times W \times H)$ $\pi/6$. Tumor growth for each day was calculated relative to the last measurement taken prior to treatment administration (day 0). Area under the curve, a tool to measure kinetics of tumor growth in experimental animals,[59] was computed using GraphPad Prism (GraphPad Software, RRID: SCR_002798, San Diego, CA).

A total of 48 h after treatment administration, blood samples (200 μL) were obtained in BD Vacutainer Plus Blood Collection tubes and centrifuged for 15 min at 2,000 × *g* to obtain serum. Complete blood count and biochemistry analysis were obtained using FUJI-DRI CHEM 4000i (FUJIFILM Corporation, Tokyo, Japan). The studies were approved by the Spanish "Animal Ethic Committees" in compliance with European Union Directives.

Tumor immune infiltration by flow cytometry

To study tumor immune infiltrate, resected CMT64 tumors were digested with collagenase IV (1 mg/mL) in agitation for 40 min at 37°C and mechanically homogenized using a Potter-Elvehjem PTFE pestle when necessary. Cell suspensions were filtered through a sterile 70-μm nylon mesh cell strainer and red blood cells were lysed by incubation with Quicklysis buffer (Cytognos, Salamanca, Spain). Pools of cell suspensions were blocked with mouse FcR Blocking (Miltenyi Biotec, Madrid, Spain) for 15 min and incubated with the following mouse mAbs for 20 min at 4°C: CD45 (30-F11), CD3 (145-2C11), CD4 (GK1.5), CD8 (53–6.7), CD11b (M1/70), CD11c (N418), CD206 (C068C2), MHCII (M5/114.15.2), Ly6C (AL-21), Ly6G (1A8-Ly6g), CD49b (DX5), and NK1.1 (PK136), all of them from eBioScience-Thermo Fisher Scientific (Waltham, MA); CD137 (1AH2PD-1) and PD-1 (29F.1A12) from BioLegend (San Diego, CA). Samples were acquired using a MACSQuant Analyzer cytometer and analyzed using MACSQuantify analysis software (Miltenyi Biotec). Density of the following immune cell populations was normalized to tumor volume to allow for comparisons: leukocytes ($CD45^+$); T cells ($CD45^+$ $CD3^+$), subclassified in Th cells ($CD4^+$) and cytotoxic T cells ($CD8^+$); NK cells ($CD45^+$ $CD11c^+$ $CD49b^+$); myeloid cells ($CD45^+$ $CD11b^+$), subclassified in monocytes ($Ly6G^-$ $MHCII^-$), macrophages ($Ly6G^-$ $MHCII^+$), and neutrophils ($Ly6G^+$ $MHCII^-$). M1/M2 and N1/N2 subsets were also considered ($CD206^-$/$CD206^+$).

NF-κB activity

A luciferase reporter system was used to evaluate the activation of NF-κB pathway *in vitro* and *in vivo*. Tumor cells were transduced overnight with a lentiviral vector based on the pHAGE NF-κB-TA-LUC-UBC-GFP-W plasmid (Addgene, plasmid cat. no. 49343) and NF-κB-Luc cells were obtained.

To study the activation of NF-κB in tumor cells, 5×10^4 NF-κB-Luc CMT64 cells were seeded overnight in 24-well plates with complete DMEM after infection with ISC301 or ICOVIR-5. Luciferase activity was assayed at different time points with the Luciferase Assay System (Promega Corporation, Madrid, Spain).

To study the *in vivo* activation of NF-κB in the tumor, 1×10^6 NF-κB-Luc CMT64 cells were implanted subcutaneously in 7-week-old C57BL/6 mice. When the tumors were measurable, a single dose of PBS, ICOVIR-5, or ISC301 was inoculated intravenously. NF-κB activation was monitored *in vivo* by luminescence imaging using the IVIS 200 system (Caliper Life Sciences, Hopkinton, MA) at for 6 days after treatment administration. Data were analyzed using Living Image software (RRID: SCR_014247; Xenogen, Alameda, CA).

Lentivirus of CAR T construct

NKG2D-41BB-CD3z construct was kindly provided by Dr. Lucia Fernandez (CNIO). This second-generation fully human CAR contains a (1) extracellular domain of NKG2D (designed by Wai-Hang Leung and Wing Leung), (2) a hinge region of CD8a, and (3) signaling domains of 4-1BB and CD3Z, as described previously.[60]

Lentiviral vectors were produced in HEK293T cells co-transfected with the NKG2D CAR encoding plasmid, packaging plasmid (PsPAX2), and envelope plasmid (VSV-G). Supernatants were collected 48 h after transfection, filtered through a 0.45-μm filter (Millipore Iberica, Madrid, Spain), and ultracentrifuged at 23,000 rpm for 2 h at 4°C (Viral Vector Production Unit, Universitat Autònoma de Barcelona, Spain).

Coculture of human CAR T cells with virus-infected tumor cells

Fresh human peripheral blood mononuclear cells (PBMCs) from healthy donors were acquired from Biobank Hospital Universitario Puerta de Hierro Majadahonda (PT17/0015/0020 by the Spanish National Biobanks Network) by leukocyte reduction system cones. From thawed PBMCs, T cells were isolated by negative selection using a Pan T cell Isolation Kit (Miltenyi Biotec), followed by incubation of X-VIVO 15 medium supplemented with IL-2 (250 U/mL; Miltenyi Biotec) and Dynabeads Human T-Activator CD3/CD28 (Gibco, Thermo Fisher Scientific) at 1:2 (bead/T cell) ratio. Next day,

activated T cells were transduced with lentiviral particles using MOI of 2. Medium was refreshed every 2–3 days and maintained at a concentration of 10^6 cells/mL. From day 7, beads were removed and medium was replaced containing IL-2 40 U/mL to CAR T cell expansion.

A549 were seeded 2×10^4 cells/well into a p24 plate. After 24 h, cells were infected with ICOVIR-5 and ISC301 as described above with MOI of 2. Two days after infection, cells were cocultured with resting CAR T- NKG2D at 1:10 (effector/target) ratio. After 24 h, cells were collected and stained with 7AAD (BioLegend) and analyzed by flow cytometry. Percentage of living tumor cells were calculated relative to control (PBS).

Statistical analysis

Data were analyzed and graphed with GraphPad Prism (GraphPad Software). *In vitro* results were expressed as mean +SD and *in vivo* results were expressed as mean ± SEM. Significant differences between two groups were determined using parametric (unpaired t test) or nonparametric (Mann-Whitney) tests according to the normality of the data (Shapiro-Wilk test). For comparison of multiple groups, ANOVA followed by Tukey multiple comparisons tests (parametric), or Kruskall-Wallis test followed by Dunn multiple comparisons tests (nonparametric), were used according to the normality of the data. $^*p < 0.05$, $^{**}p < 0.01$, and $^{***}p < 0.001$ were deemed statistically significant.

DATA AND CODE AVAILABILITY

The data that support the findings of this study are available from the corresponding author upon reasonable request.

ACKNOWLEDGMENTS

ΔP-L2 plasmid was kindly provided from Dr. Mizuguchi (National Institutes of Health Sciences, Tokyo, Japan); NKG2D-41BB-CD3z construct was kindly provided by Dr. Lucia Fernandez (CNIO, Madrid, Spain). We also thank Daniel Luque and Carmen Terrón for their assistance with TEM images. This study was funded by Instituto de Salud Carlos III: grants PI17CIII/00013, PI20CIII-00040, and PI23CIII/00024, RICORS-Red Española de Terapias Avanzadas TERAV ISCIII (RD21/0017/0005), NextGenerationEU funded. Plan de Recuperación Transformación y Resiliencia, Plan Estatal de Investigación Científica, Técnica y de Innovación (grant RED2022-134221-T), Consejería de Educación, Juventud y Deporte de la Comunidad de Madrid (NEXT_GEN_CART_MADCM; grant P2022/BMD7225), Fundación Oncohematología Infantil, AFANION and Asociación Pablo Ugarte, whose support we gratefully acknowledge. P.G.-R. is a beneficiary of PhD ISCIII-PFIS program (FI22CIII/00004) and enrolling in the Doctoral Program in Biomedical Sciences and Public Health as a predoctoral researcher at the UNED International Doctoral School. L.H. was beneficiary of a grant under the Talent Attraction Program of the Comunidad de Madrid (2018-T2/BMD-10337).

AUTHOR CONTRIBUTIONS

Investigation, A.M.-M., M.A.R.-M., P.G.-R., L.H., and J.G.-C.; methodology, A.M.-M., M.A.R.-M., P.G.-R., L.H., and J.G.-C.; formal analysis, A.M.-M.; data curation, A.M.-M.; validation, A.M.-M., M.A.R.-M., P.G.-R., L.H., and R.A.; visualization. A.M.-M.; writing – original draft, A.M.-M., M.A.R.-M., and J.G.-C.; writing – review & editing, A.M.-M., M.A.R.-M., P.G.-R., L.H., R.A., and J.G.-C.; conceptualization, R.A. and J.G.-C.; resources, R.A. and J.G.-C.; funding acquisition, J.G.-C.; supervision, J.G.-C.; project administration, J.G.-C.

DECLARATION OF INTERESTS

The authors declare no competing interests.

SUPPLEMENTAL INFORMATION

Supplemental information can be found online at https://doi.org/10.1016/j.omton.2024.200863.

REFERENCES

1. Hamid, O., Hoffner, B., Gasal, E., Hong, J., and Carvajal, R.D. (2017). Oncolytic immunotherapy: unlocking the potential of viruses to help target cancer. Cancer Immunol. Immunother. *66*, 1249–1264. https://doi.org/10.1007/s00262-017-2025-8.

2. Jiang, H., Rivera-Molina, Y., Gomez-Manzano, C., Clise-Dwyer, K., Bover, L., Vence, L.M., Yuan, Y., Lang, F.F., Toniatti, C., Hossain, M.B., and Fueyo, J. (2017). Oncolytic Adenovirus and Tumor-Targeting Immune Modulatory Therapy Improve Autologous Cancer Vaccination. Cancer Res. *77*, 3894–3907. https://doi.org/10.1158/0008-5472.can-17-0468.

3. Einhorn, L.H., Bond, W.H., Hornback, N., and Joe, B.T. (1978). Long-term results in combined-modality treatment of small cell carcinoma of the lung. Semin. Oncol. *5*, 309–313. https://doi.org/10.1200/jco.2002.08.092.

4. Essential drugs for cancer chemotherapy: memorandum from a WHO meeting (1985). Bull. World Health Organ. *63*, 999–1002.

5. Morrissey, K.M., Yuraszeck, T.M., Li, C.C., Zhang, Y., and Kasichayanula, S. (2016). Immunotherapy and Novel Combinations in Oncology: Current Landscape, Challenges, and Opportunities. Clin. Transl. Sci. *9*, 89–104. https://doi.org/10.1111/cts.12391.

6. Tian, Y., Xie, D., and Yang, L. (2022). Engineering strategies to enhance oncolytic viruses in cancer immunotherapy. Signal Transduct. Targeted Ther. *7*, 117. https://doi.org/10.1038/s41392-022-00951-x.

7. Rezaei, R., Esmaeili Gouvarchin Ghaleh, H., Farzanehpour, M., Dorostkar, R., Ranjbar, R., Bolandian, M., Mirzaei Nodooshan, M., and Ghorbani Alvanegh, A. (2022). Combination therapy with CAR T cells and oncolytic viruses: a new era in cancer immunotherapy. Cancer Gene Ther. *29*, 647–660. https://doi.org/10.1038/s41417-021-00359-9.

8. Cascallo, M., Alonso, M.M., Rojas, J.J., Perez-Gimenez, A., Fueyo, J., and Alemany, R. (2007). Systemic toxicity-efficacy profile of ICOVIR-5, a potent and selective oncolytic adenovirus based on the pRB pathway. Mol. Ther. *15*, 1607–1615. https://doi.org/10.1038/sj.mt.6300239.

9. Alonso, M.M., Cascallo, M., Gomez-Manzano, C., JIang, H., Bekele, B.N., Perez-Gimenez, A., Lang, F.F., Piao, Y., Alemany, R., and Fueyo, J. (2007). ICOVIR-5 shows E2F1 addiction and potent antiglioma effect in vivo. Cancer Res. *67*, 8255–8263. https://doi.org/10.1158/0008-5472.can-06-4675.

10. Laborda, E., Puig-Saus, C., Rodriguez-García, A., Moreno, R., Cascalló, M., Pastor, J., and Alemany, R. (2014). A pRb-responsive, RGD-modified, and hyaluronidase-armed canine oncolytic adenovirus for application in veterinary oncology. Mol. Ther. *22*, 986–998. https://doi.org/10.1038/mt.2014.7.

11. Ramirez, M., Ruano, D., Moreno, L., Lassaletta, Á., Sirvent, F.J.B., Andión, M., Hernández, C., González-Murillo, Á., Melen, G., Alemany, R., et al. (2018). First-in-child trial of celyvir (autologous mesenchymal stem cells carrying the oncolytic virus ICOVIR-5) in patients with relapsed and refractory pediatric solid tumors. J. Clin. Oncol. *36*, 10543. https://doi.org/10.1200/JCO.2018.36.15_suppl.10543.

12. Cejalvo, T., Perisé-Barrios, A.J., Del Portillo, I., Laborda, E., Rodriguez-Milla, M.A., Cubillo, I., Vázquez, F., Sardón, D., Ramirez, M., Alemany, R., et al. (2018). Remission of Spontaneous Canine Tumors after Systemic Cellular Viroimmunotherapy. Cancer Res. *78*, 4891–4901. https://doi.org/10.1158/0008-5472.can-17-3754.

13. Ruano, D., López-Martín, J.A., Moreno, L., Lassaletta, Á., Bautista, F., Andión, M., Hernández, C., González-Murillo, Á., Melen, G., Alemany, R., et al. (2020). First-in-Human, First-in-Child Trial of Autologous MSCs Carrying the Oncolytic Virus Icovir-5 in Patients with Advanced Tumors. Mol. Ther. *28*, 1033–1042. https://doi.org/10.1016/j.ymthe.2020.01.019.

14. Rodríguez-Milla, M.Á., Morales-Molina, A., Perisé-Barrios, A.J., Cejalvo, T., and García-Castro, J. (2021). AKT and JUN are differentially activated in mesenchymal stem cells after infection with human and canine oncolytic adenoviruses. Cancer Gene Ther. *28*, 64–73. https://doi.org/10.1038/s41417-020-0184-9.

15. Keriel, A., René, C., Galer, C., Zabner, J., and Kremer, E.J. (2006). Canine adenovirus vectors for lung-directed gene transfer: efficacy, immune response, and duration of

transgene expression using helper-dependent vectors. J. Virol. *80*, 1487–1496. https://doi.org/10.1128/jvi.80.3.1487-1496.2006.

16. Fejer, G., Freudenberg, M., Greber, U.F., and Gyory, I. (2011). Adenovirus-triggered innate signalling pathways. Eur. J. Microbiol. Immunol. *1*, 279–288. https://doi.org/10.1556/EuJMI.1.2011.4.3.

17. Greber, U.F., and Flatt, J.W. (2019). Adenovirus Entry: From Infection to Immunity. Annu. Rev. Virol. *6*, 177–197. https://doi.org/10.1146/annurev-virology-092818-015550.

18. Greber, U.F. (2002). Signalling in viral entry. Cell. Mol. Life Sci. *59*, 608–626. https://doi.org/10.1007/s00018-002-8453-3.

19. Soudais, C., Boutin, S., Hong, S.S., Chillon, M., Danos, O., Bergelson, J.M., Boulanger, P., and Kremer, E.J. (2000). Canine adenovirus type 2 attachment and internalization: coxsackievirus-adenovirus receptor, alternative receptors, and an RGD-independent pathway. J. Virol. *74*, 10639–10649. https://doi.org/10.1128/jvi.74.22.10639-10649.2000.

20. Albinsson, B., and Kidd, A.H. (1999). Adenovirus type 41 lacks an RGD alpha(v)-integrin binding motif on the penton base and undergoes delayed uptake in A549 cells. Virus Res. *64*, 125–136. https://doi.org/10.1016/s0168-1702(99)00087-8.

21. Shayakhmetov, D.M., Eberly, A.M., Li, Z.Y., and Lieber, A. (2005). Deletion of penton RGD motifs affects the efficiency of both the internalization and the endosome escape of viral particles containing adenovirus serotype 5 or 35 fiber knobs. J. Virol. *79*, 1053–1061. https://doi.org/10.1128/jvi.79.2.1053-1061.2005.

22. Philpott, N.J., Nociari, M., Elkon, K.B., and Falck-Pedersen, E. (2004). Adenovirus-induced maturation of dendritic cells through a PI3 kinase-mediated TNF-alpha induction pathway. Proc. Natl. Acad. Sci. USA *101*, 6200–6205. https://doi.org/10.1073/pnas.0308368101.

23. Di Paolo, N.C., Miao, E.A., Iwakura, Y., Murali-Krishna, K., Aderem, A., Flavell, R.A., Papayannopoulou, T., and Shayakhmetov, D.M. (2009). Virus binding to a plasma membrane receptor triggers interleukin-1 alpha-mediated proinflammatory macrophage response in vivo. Immunity *31*, 110–121. https://doi.org/10.1016/j.immuni.2009.04.015.

24. Zou, X.H., Li, W.J., Guo, X.J., Qu, J.G., Wang, M., Si, H.L., Lu, Z.Z., and Hung, T. (2014). Inefficient export of viral late mRNA contributes to fastidiousness of human adenovirus type 41 (HAdV-41) in 293 cells. Virology *468–470*, 388–396. https://doi.org/10.1016/j.virol.2014.08.027.

25. Rincon, E., Cejalvo, T., Kanojia, D., Alfranca, A., Rodríguez-Milla, M.Á., Gil, R.A., Han, Y., Zhang, L., Alemany, R., Lesniak, M.S., et al. (2017). Mesenchymal stem cell carriers enhance antitumor efficacy of oncolytic adenoviruses in an immunocompetent mouse model. Oncotarget *8*, 45415–45431. https://doi.org/10.18632/oncotarget.17557.

26. Morales-Molina, Á., Gambera, S., Cejalvo, T., Moreno, R., Rodríguez-Milla, M.Á., Perisé-Barrios, A.J., and García-Castro, J. (2018). Antitumor virotherapy using syngeneic or allogeneic mesenchymal stem cell carriers induces systemic immune response and intratumoral leukocyte infiltration in mice. Cancer Immunol. Immunother. *67*, 1589–1602. https://doi.org/10.1007/s00262-018-2220-2.

27. Morales-Molina, A., Rodriguez-Milla, M.Á., Gambera, S., Cejalvo, T., de Andrés, B., Gaspar, M.L., and García-Castro, J. (2023). Toll-like Receptor Signaling-deficient Cells Enhance Antitumor Activity of Cell-based Immunotherapy by Increasing Tumor Homing. Cancer Res. Commun. *3*, 347–360. https://doi.org/10.1158/2767-9764.crc-22-0365.

28. Hidalgo, L., Somovilla-Crespo, B., Garcia-Rodriguez, P., Morales-Molina, A., Rodriguez-Milla, M.A., and Garcia-Castro, J. (2023). Switchable CAR T cell strategy against osteosarcoma. Cancer Immunol. Immunother. *72*, 2623–2633. https://doi.org/10.1007/s00262-023-03437-z.

29. Andtbacka, R.H.I., Kaufman, H.L., Collichio, F., Amatruda, T., Senzer, N., Chesney, J., Delman, K.A., Spitler, L.E., Puzanov, I., Agarwala, S.S., et al. (2015). Talimogene Laherparepvec Improves Durable Response Rate in Patients With Advanced Melanoma. J. Clin. Oncol. *33*, 2780–2788. https://doi.org/10.1200/jco.2014.58.3377.

30. Todo, T., Ito, H., Ino, Y., Ohtsu, H., Ota, Y., Shibahara, J., and Tanaka, M. (2022). Intratumoral oncolytic herpes virus G47Δ for residual or recurrent glioblastoma: a phase 2 trial. Nat. Med. *28*, 1630–1639. https://doi.org/10.1038/s41591-022-01897-x.

31. Oncorine, L.M. (2018). the World First Oncolytic Virus Medicine and its Update in China. Curr. Cancer Drug Targets *18*, 171–176. https://doi.org/10.2174/1568009618666171129221503.

32. Shalhout, S.Z., Miller, D.M., Emerick, K.S., and Kaufman, H.L. (2023). Therapy with oncolytic viruses: progress and challenges. Nat. Rev. Clin. Oncol. *20*, 160–177. https://doi.org/10.1038/s41571-022-00719-w.

33. Blanchette, P., and Teodoro, J.G. (2023). A Renaissance for Oncolytic Adenoviruses? Viruses *15*, 358. https://doi.org/10.3390/v15020358.

34. Tripodi, L., Vitale, M., Cerullo, V., and Pastore, L. (2021). Oncolytic Adenoviruses for Cancer Therapy. Int. J. Mol. Sci. *22*, 2517. https://doi.org/10.3390/ijms22052517.

35. Zubieta, C., Schoehn, G., Chroboczek, J., and Cusack, S. (2005). The structure of the human adenovirus 2 penton. Mol. Cell. *17*, 121–135. https://doi.org/10.1016/j.molcel.2004.11.041.

36. Liu, Q., Zaiss, A.K., Colarusso, P., Patel, K., Haljan, G., Wickham, T.J., and Muruve, D.A. (2003). The role of capsid-endothelial interactions in the innate immune response to adenovirus vectors. Hum. Gene Ther. *14*, 627–643. https://doi.org/10.1089/104303403321618146.

37. Dmitriev, I., Krasnykh, V., Miller, C.R., Wang, M., Kashentseva, E., Mikheeva, G., Belousova, N., and Curiel, D.T. (1998). An adenovirus vector with genetically modified fibers demonstrates expanded tropism via utilization of a coxsackievirus and adenovirus receptor-independent cell entry mechanism. J. Virol. *72*, 9706–9713. https://doi.org/10.1128/jvi.72.12.9706-9713.1998.

38. Hendrickx, R., Stichling, N., Koelen, J., Kuryk, L., Lipiec, A., and Greber, U.F. (2014). Innate immunity to adenovirus. Hum. Gene Ther. *25*, 265–284. https://doi.org/10.1089/hum.2014.001.

39. Ozes, O.N., Mayo, L.D., Gustin, J.A., Pfeffer, S.R., Pfeffer, L.M., and Donner, D.B. (1999). NF-kappaB activation by tumour necrosis factor requires the Akt serine-threonine kinase. Nature *401*, 82–85. https://doi.org/10.1038/43466.

40. Romashkova, J.A., and Makarov, S.S. (1999). NF-kappaB is a target of AKT in anti-apoptotic PDGF signalling. Nature *401*, 86–90. https://doi.org/10.1038/43474.

41. Liu, Q., and Muruve, D.A. (2003). Molecular basis of the inflammatory response to adenovirus vectors. Gene Ther. *10*, 935–940. https://doi.org/10.1038/sj.gt.3302036.

42. Liu, Q., White, L.R., Clark, S.A., Heffner, D.J., Winston, B.W., Tibbles, L.A., and Muruve, D.A. (2005). Akt/protein kinase B activation by adenovirus vectors contributes to NFkappaB-dependent CXCL10 expression. J. Virol. *79*, 14507–14515. https://doi.org/10.1128/jvi.79.23.14507-14515.2005.

43. Zhu, J., Huang, X., and Yang, Y. (2007). Innate immune response to adenoviral vectors is mediated by both Toll-like receptor-dependent and -independent pathways. J. Virol. *81*, 3170–3180. https://doi.org/10.1128/jvi.02192-06.

44. Raman, S., Hsu, T.H., Ashley, S.L., and Spindler, K.R. (2009). Usage of integrin and heparan sulfate as receptors for mouse adenovirus type 1. J. Virol. *83*, 2831–2838. https://doi.org/10.1128/jvi.02368-08.

45. Teigler, J.E., Kagan, J.C., and Barouch, D.H. (2014). Late endosomal trafficking of alternative serotype adenovirus vaccine vectors augments antiviral innate immunity. J. Virol. *88*, 10354–10363. https://doi.org/10.1128/jvi.00936-14.

46. Teigler, J.E., Iampietro, M.J., and Barouch, D.H. (2012). Vaccination with adenovirus serotypes 35, 26, and 48 elicits higher levels of innate cytokine responses than adenovirus serotype 5 in rhesus monkeys. J. Virol. *86*, 9590–9598. https://doi.org/10.1128/jvi.00740-12.

47. Atasheva, S., and Shayakhmetov, D.M. (2022). Cytokine Responses to Adenovirus and Adenovirus Vectors. Viruses *14*, 888. https://doi.org/10.3390/v14050888.

48. Smith, J.G., Silvestry, M., Lindert, S., Lu, W., Nemerow, G.R., and Stewart, P.L. (2010). Insight into the mechanisms of adenovirus capsid disassembly from studies of defensin neutralization. PLoS Pathog. *6*, e1000959. https://doi.org/10.1371/journal.ppat.1000959.

49. Smith, J.G., and Nemerow, G.R. (2008). Mechanism of adenovirus neutralization by Human alpha-defensins. Cell Host Microbe *3*, 11–19. https://doi.org/10.1016/j.chom.2007.12.001.

50. Atasheva, S., Yao, J., and Shayakhmetov, D.M. (2019). Innate immunity to adenovirus: lessons from mice. FEBS Lett. *593*, 3461–3483. https://doi.org/10.1002/1873-3468.13696.

51. Galon, J., and Bruni, D. (2019). Approaches to treat immune hot, altered and cold tumours with combination immunotherapies. Nat. Rev. Drug Discov. *18*, 197–218. https://doi.org/10.1038/s41573-018-0007-y.

52. Kankeu Fonkoua, L.A., Sirpilla, O., Sakemura, R., Siegler, E.L., and Kenderian, S.S. (2022). CAR T cell therapy and the tumor microenvironment: Current challenges and opportunities. Mol. Ther. Oncolytics *25*, 69–77. https://doi.org/10.1016/j.omto.2022.03.009.

53. Liu, H., Wang, S., Xin, J., Wang, J., Yao, C., and Zhang, Z. (2019). Role of NKG2D and its ligands in cancer immunotherapy. Am. J. Cancer Res. *9*, 2064–2078.

54. Zhu, J., Huang, X., and Yang, Y. (2010). NKG2D is required for NK cell activation and function in response to E1-deleted adenovirus. J. Immunol. *185*, 7480–7486. https://doi.org/10.4049/jimmunol.1002771.

55. Chen, P.H., Lipschitz, M., Weirather, J.L., Jacobson, C., Armand, P., Wright, K., Hodi, F.S., Roberts, Z.J., Sievers, S.A., Rossi, J., et al. (2020). Activation of CAR and non-CAR T cells within the tumor microenvironment following CAR T cell therapy. JCI Insight *5*, e134612. https://doi.org/10.1172/jci.insight.134612.

56. Wang, C., Zeng, Q., Gül, Z.M., Wang, S., Pick, R., Cheng, P., Bill, R., Wu, Y., Naulaerts, S., Barnoud, C., et al. (2024). Circadian tumor infiltration and function of CD8(+) T cells dictate immunotherapy efficacy. Cell *187*, 2690–2702.e17. https://doi.org/10.1016/j.cell.2024.04.015.

57. Mamola, J.A., Chen, C.Y., Currier, M.A., Cassady, K., Lee, D.A., and Cripe, T.P. (2023). Opportunities and challenges of combining adoptive cellular therapy with oncolytic virotherapy. Mol. Ther. Oncolytics *29*, 118–124. https://doi.org/10.1016/j.omto.2023.04.008.

58. Mizuguchi, H., Koizumi, N., Hosono, T., Ishii-Watabe, A., Uchida, E., Utoguchi, N., Watanabe, Y., and Hayakawa, T. (2002). CAR- or alphav integrin-binding ablated adenovirus vectors, but not fiber-modified vectors containing RGD peptide, do not change the systemic gene transfer properties in mice. Gene Ther. *9*, 769–776. https://doi.org/10.1038/sj.gt.3301701.

59. Duan, F., Simeone, S., Wu, R., Grady, J., Mandoiu, I., and Srivastava, P.K. (2012). Area under the curve as a tool to measure kinetics of tumor growth in experimental animals. J. Immunol. Methods *382*, 224–228. https://doi.org/10.1016/j.jim.2012.06.005.

60. Fernández, L., Metais, J.Y., Escudero, A., Vela, M., Valentín, J., Vallcorba, I., Leivas, A., Torres, J., Valeri, A., Patiño-García, A., et al. (2017). Memory T Cells Expressing an NKG2D-CAR Efficiently Target Osteosarcoma Cells. Clin. Cancer Res. *23*, 5824–5835. https://doi.org/10.1158/1078-0432.ccr-17-0075.

OMTON, Volume *32*

Supplemental information

Deletion of the RGD motif from the penton base in oncolytic adenoviruses enhances antitumor efficacy of combined CAR T cell therapy

Alvaro Morales-Molina, Miguel Angel Rodriguez-Milla, Patricia Garcia-Rodriguez, Laura Hidalgo, Ramon Alemany, and Javier Garcia-Castro

Figure S1

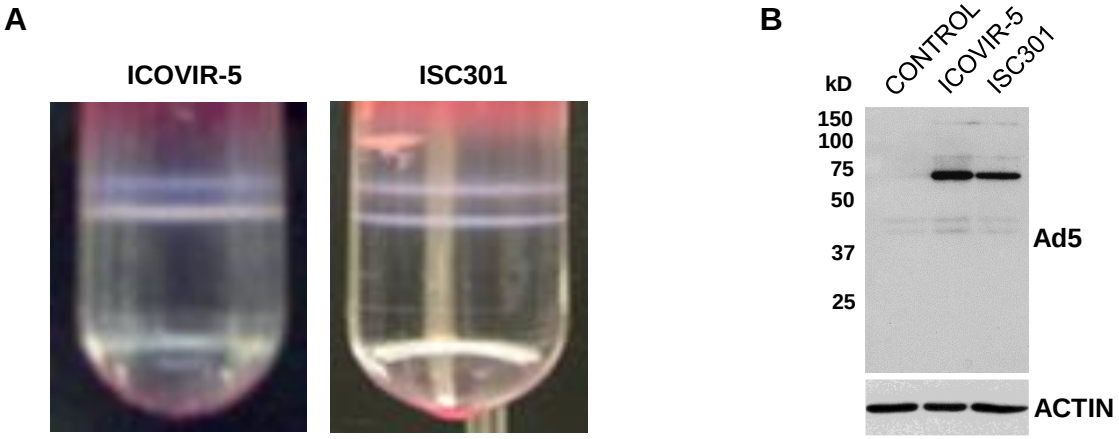

Figure S1. Development of a novel human oncolytic adenovirus. A, Purification of ICOVIR-5 and ISC301 in HEK293 cells by CsCl density gradient showing bands of mature virions (lower) and empty capsids (top). **B,** Western blot analysis showing the expression of adenoviral proteins in CMT64 cells infected for 24 h with ICOVIR-5 and ISC301 (200 PFU/cell). Actin was used as a loading control.

Figure S2

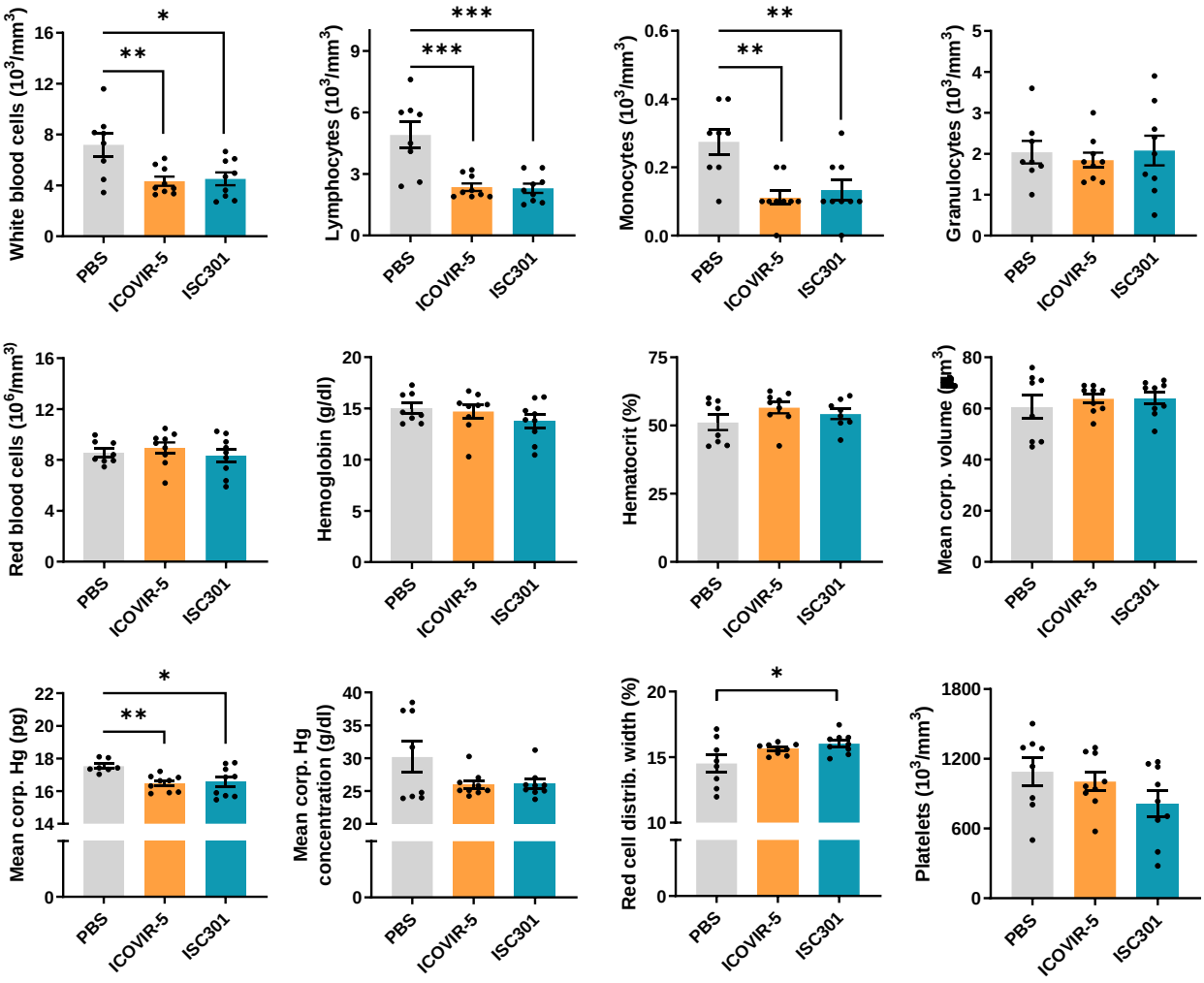

Figure S2. Immune cell populations in peripheral blood 48 h after treatment administration. Complete blood count and parameters studied at 48 h after administration of PBS (grey), ICOVIR-5 (yellow) and ISC301 (blue); n = 8-9. One-way ANOVA followed by Tukey's multiple comparisons tests. *p < 0.05, **p < 0.01, ***p < 0.001.

Figure S3

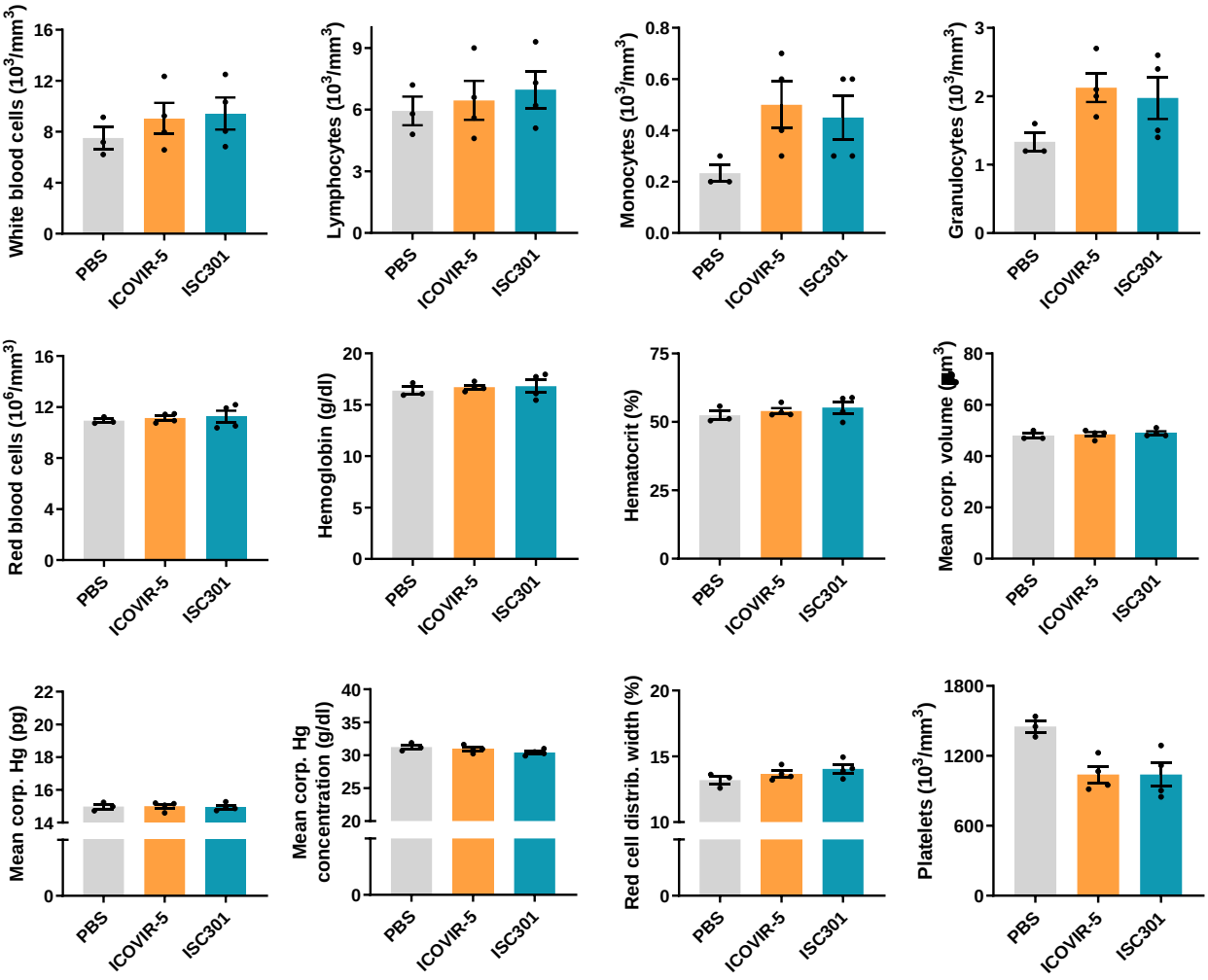

Figure S3. Immune cell populations in peripheral blood 11 days after treatment administration. Complete blood count and parameters studied at 11 days after administration of PBS (grey), ICOVIR-5 (yellow) and ISC301 (blue); n = 3-4. One-way ANOVA followed by Tukey's multiple comparisons tests.